Carbohydrate Polymer Technologies and Applications 9 (2025) 100731

Contents lists available at ScienceDirect

Carbohydrate Polymer Technologies and Applications

journal homepage: www.sciencedirect.com/journal/carbohydrate-polymer-technologies-and-applications

Cellulose oligomer synthesis: Primer effects on structural characteristics in the cellodextrin phosphorylase-catalyzed reverse reaction

Tatsuhiro Konishi [a], Atsushi Sasaki [a], Ryosuke Kusumi [b], Masahisa Wada [a], Kayoko Kobayashi [a,*]

[a] Division of Forest and Biomaterials Science, Graduate School of Agriculture, Kyoto University, Kitashirakawa-oiwakecho, Sakyo-ku, Kyoto, 606-8502, Japan
[b] Department of Forest Resource Chemistry, Forestry and Forest Products Research Institute, 1 Matsunosato, Tsukuba, 305-8687, Japan

ARTICLE INFO

Keywords:
Cellodextrin phosphorylase-catalyzed reverse reaction
Cellulose oligomers
Molecular weight distribution
Cellobiose
Oligomer crystal structure
Chemical structures of synthetic cellulose oligomers

ABSTRACT

The synthesis of cellulose oligomers catalyzed by cellodextrin phosphorylase (CDP) can easily yield microcrystals with functional groups exposed on their surfaces using glucose derivatives with various functional groups at the C1 position as primers. In this study, we examined and compared the effects of primers with various structures on the structural characteristics of the resulting synthetic products. The yield of the synthetic products positively correlated with the CDP activity toward the primer, whereas the degree of polymerization (DP) and molecular weight distribution showed an inverse correlation. However, deviations from these trends were observed, suggesting the influence of varying solubilities and crystallization behaviors due to the introduction of functional groups. The obtained microcrystals exhibited a primarily plate-like shape with a thickness increasing in proportion to the DP, resulting in larger plate-like crystals at higher DP values. These findings provide insights into strategies for controlling the structure of the resulting cellulose oligomers.

1. Introduction

Cellulose oligomers can be synthesized via a reverse reaction catalyzed by cellodextrin phosphorylase (CDP, EC 2.4.1.49) (Arai et al., 1994; Hiraishi et al., 2009; Samain et al., 1995; Serizawa et al., 2016). As cellulose chains elongate, cellulose oligomers become increasingly insoluble in water, typically forming lamellar crystals in the cellulose II crystalline form with cellulose chains having a degree of polymerization (DP) of 7–10, arranged orthogonally to the lamellar plane (Hiraishi et al., 2009; Serizawa et al., 2016). Unlike other cellulose synthesis methods, such as chemical synthesis (Guberman & Seeberger, 2019; Nakatsubo et al., 1996) and glycosynthase synthesis (Kobayashi et al., 1991), CDP synthesis can be achieved through a simple process using commercially available chemicals. When combined with phosphoric acid hydrolysis of sucrose catalyzed by sucrose phosphorylase (SP) to produce glucose-1-phosphate (G1P), cellulose oligomers can be synthesized using sucrose and primers (Kita et al., 2020) (Fig. 1a). Thus, sufficient quantities of products can be obtained for various analyses and applications. Another unique aspect of CDP synthesis is its compatibility with various primers, owing to the low substrate specificity of CDP (Samain et al., 1995). Consequently, cellulose oligomers with functional groups at their reducing ends can be readily obtained without the need of additional chemical reactions (Fig. 1b).

CDP is an enzyme that degrades cellulose oligomers longer than cellobiose via phosphorolysis (Sheth & Alexander, 1969). Cellobiose and cellulose oligomers have been used as primers for reverse reactions and CDP synthesis (Krishnareddy et al., 2002; Zhang & Lynd, 2004). Cellobiose derivatives with functional groups at their reducing end, such as methyl β-cellobioside and phenyl β-cellobioside, have also been reported as effective primers for CDP synthesis, demonstrating equal or greater CDP activity toward these cellobiosides than that toward cellobiose (Samain et al., 1995). Because CDP does not exhibit glucose activity, it

List of abbreviations: CDP, cellodextrin phosphorylase; DP, degree of polymerization; SP, sucrose phosphorylase; G1P, glucose-1-phosphate; NMR, nuclear magnetic resonance; FT-IR, Fourier-transform infrared; DMSO, dimethylsulfoxide; MALDI-TOF MS, matrix-assisted laser desorption/ionization time-of-flight mass spectrometry; TEM, transmission electron microscopy; AFM, atomic force microscopy; SAXS, small-angle X-ray scattering; WAXD, wide-angle X-ray diffraction; TOCSY, total correlation spectroscopy; DPn, number-averaged degree of polymerization; Mn, number-average molecular weight; Mw, weight-average molecular weight.

* Corresponding author.
E-mail addresses: konishi.tatsuhiro.g27@kyoto-u.jp (T. Konishi), sasaki.atsushi.v78@kyoto-u.jp (A. Sasaki), rkusumi@ffpri.affrc.go.jp (R. Kusumi), wada.masahisa.8c@kyoto-u.ac.jp (M. Wada), kobayashi.kayoko.3s@kyoto-u.ac.jp (K. Kobayashi).

https://doi.org/10.1016/j.carpta.2025.100731

Available online 24 February 2025

was initially postulated that synthesizing cello-oligosaccharides using glucose as a primer was not feasible. However, Hiraishi et al. (2009) reported the applicability of glucose as a primer, albeit with significantly lower activity compared to cellobiose and cellulose oligomers. Subsequently, several studies have synthesized cellulose oligomers from glucose and its derivatives bearing functional groups at their reducing end (Adharis et al., 2018; de Andrade et al., 2021; Nohara et al., 2017; Pylkkänen et al., 2024; Sugiura et al., 2022; Wang et al., 2022; Yataka et al., 2015, 2016; Zhong & Nidetzky, 2022).

The DP of cellulose oligomers synthesized from glucose was higher than that of those synthesized from cellobiose (Hiraishi et al., 2009; Serizawa et al., 2017) owing to the reactivity of CDP. When cellobiose was used as the primer, all cellulose chains extended equally from both cellobiose and longer oligomers. In contrast, when glucose was used as the primer, only a small fraction of glucose molecules extended to form cellobiose, which preferentially acted as an acceptor and continued to elongate. The effects of reaction temperature and substrate concentrations on the DP and yields of synthetic cellulose oligomers have also been investigated (Hata et al., 2019; Petrović et al., 2015; Pylkkänen et al., 2020). The resulting crystal structures varied depending on the primers used. In particular, the use of glucose derivatives with alkyl chains as primers resulted in the formation of cellulose I crystals with characteristic twisted shapes (Serizawa et al., 2021; Yataka et al., 2016). However, the structural characteristics of the products and the underlying mechanisms remain unclear when using primers with various functional groups.

Herein, we report the effects of different primers on the DP of the resulting synthetic products and their solid-state structures. As the functional groups at the reducing ends of the primers are exposed on the lamellar surface of the synthetic cellulose oligomers, these functional groups can be utilized in various ways. For example, the introduction of azido groups provides water dispersibility (Wada et al., 2021) and enables additional functionalities, including initiating chemical reactions, such as click chemistry (Yataka et al., 2015). Other studies have suggested the potential for controlling higher-order structures via alkyl group introduction (Serizawa et al., 2021; Yataka et al., 2016) and bio-utilization via amino group introduction (Nohara et al., 2017; Serizawa et al., 2024). Because methods for obtaining homogeneous cellulose oligomers are limited, cellulose oligomers obtained by CDP synthesis are useful model substances for fundamental research on cellulose structure and dissolution (Kita et al., 2020; Sasaki et al., 2024). Therefore, cellulose oligomers obtained via CDP synthesis are expected to have various applications. The utility of cellulose oligomers can be further expanded by controlling the DP and solid-state structures using primers.

2. Materials and methods

2.1. Primer structures

We used 10 primers (Fig. 2), namely d-glucose (**1**), d-cellobiose (**2**), methyl α-d-glucopyranoside (**3**), methyl β-d-glucopyranoside (**4**), hexyl β-d-glucopyranoside (**5**), phenyl β-d-glucopyranoside (**6**), 4-hydroxyphenyl β-d-glucopyranoside (**7**), 4-nitrophenyl β-d-glucopyranoside (**8**), 1-azido-1-deoxy β-d-glucopyranoside (**9**), and d-glucono-1,5-lactone (**10**). Primers **1, 2,** and **6** were purchased from Fujifilm Wako Pure Chemical Corporation (Japan). Primers **3, 4, 7, 8,** and **10** were purchased from Tokyo Chemical Industry (Japan). Primer **5** was purchased from Biosynth Ltd. (UK), and primer **9** was purchased from Sigma-Aldrich (USA).

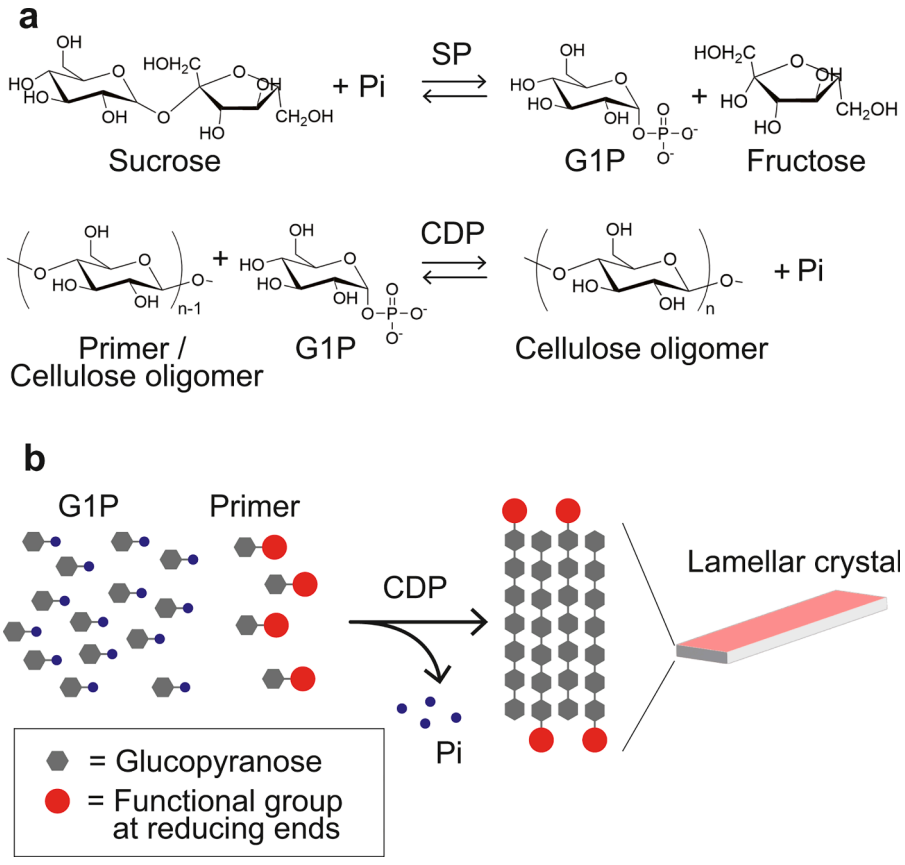

Fig. 1. (a) Schematic representation of cellulose oligomer synthesis. Sucrose is hydrolyzed by SP in the presence of phosphoric acid to produce G1P, which is subsequently utilized by CDP for cellulose oligomer synthesis in the presence of primers. (b) Schematic of CDP synthesis of cellulose oligomers bearing functional groups at their reducing ends.

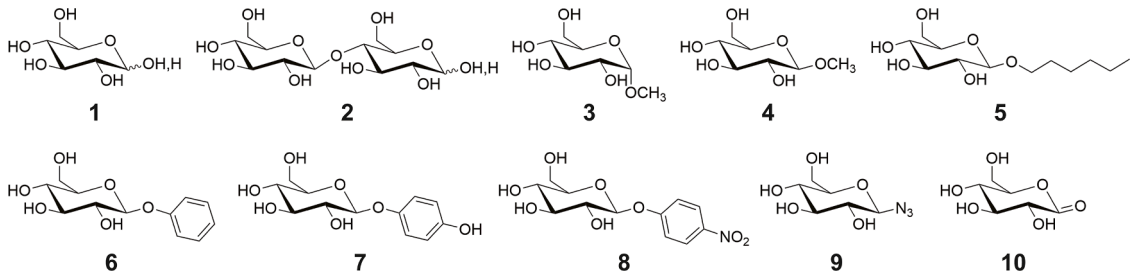

Fig. 2. Chemical structures of the primers investigated in this study.

Primers **1** and **2** were selected as standards for low and high CDP activity, respectively. Primers **3** and **4** were included to compare α- and β-anomers. Primer **5** was selected to compare the alkyl chain length with that of primer **4** and because of the unique cellulose I structure of its product. Primers **6, 7**, and **8** contained aromatic rings with different functional groups (at the para position for primers **7** and **8)**. Primer **8** is also known to serve as a substrate for the measurement of β-glucosidase activity. Primers **9** and **10** were glucose derivatives, with their functional groups directly linked to the C1 carbon. Primer **9** has been investigated in previous studies (Wada et al., 2021; Yataka et al., 2015).

Primers **1** and **2** were expected to yield standard cellulose oligomers, whereas the other primers were anticipated to generate cellulose oligomers with functional groups at their reducing ends (Fig. 1). These structural predictions were later confirmed through experimental analysis.

2.2. Synthesis of cellulose oligomers from primers

Recombinant CDP originating from the *Clostridium thermocellum* YM4 strain expressed in *Escherichia coli* was prepared and purified using a previously described method (Krishnareddy et al., 2002). A mixture of 50 mM primer, 400 mM sucrose, 50 mM phosphate buffer (pH 7.0), 0.05 U/mL CDP, and 0.2 U/mL SP was incubated at 40 °C for 3 days. The total volumes of the mixtures were 30–40 mL. The precipitate was collected by centrifugation and repeatedly washed with water to remove any residual primers and short oligomers that were soluble in water. An aliquot of the purified sample was dispersed in water for microscopic and X-ray analyses. The remaining samples were freeze dried, followed by vacuum drying at 70 °C for further measurements.

2.3. Assay of primer CDP activity

The CDP activity of the primers was evaluated using an assay based on the determination of inorganic phosphate (Pi) released in a reaction mixture containing the primer and G1P. A mixture (5 mL) of 20 mM primer, 20 mM αG1P disodium salt tetrahydrate, 50 mM 3-(N-morpholino)propanesulfonic acid buffer (pH 7.6), and 0.1 U/mL CDP was incubated at 40 °C for 30 mins. The assay for detecting inorganic phosphate in the reaction mixture was performed according to a previously reported protocol (Saheki et al., 1985), using a UV–Vis spectrometer (UV-2450, Shimadzu, Japan).

2.4. Nuclear magnetic resonance (NMR) and fourier-transform infrared (FT-IR) spectroscopy

NMR measurements were performed using a 500 MHz NMR spectrometer (Varian Inc., USA). In 0.7 mL dimethylsulfoxide (DMSO)-d_6 containing 20 mg LiCl, 40 mg of each sample were dissolved at 23 °C. Tetramethylsilane was used as the internal standard. The ^{1}H NMR spectra were obtained by setting the ^{1}H flip angle, delay time, and number of scans to 45°, 1.5 s, and 16, respectively. The FT-IR spectra of the freeze-dried samples were obtained in attenuated total reflection mode using an FT-IR spectrometer (Spectrum 3, Perkin Elmer). Measurements were performed between 4000 and 400 cm^{-1}, and 16 scans were recorded at a resolution of 4 cm^{-1}.

2.5. Matrix-assisted laser desorption/ionization time-of-flight mass spectrometry (MALDI-TOF MS)

A suspension of a cellulose oligomer (0.2 wt%) was mixed with 2,5-dihydroxybenzoic acid (Tokyo Chemical Industry Co., Ltd., Japan) saturated in 0.4 % (v/v) trifluoroacetic acid/acetonitrile at a volume ratio of either 1:1 or 1:3. The measurements were performed using a MALDI-TOF MS system (Autoflex III, Bruker Daltonics). The spectra were calibrated using the Bruker peptide standard II (Bruker Daltonics). The standard was dissolved in 0.1 % (v/v) trifluoroacetic acid/acetonitrile and mixed with an equal amount of α-cyano-4-hydroxycinnamic acid saturated in acetone.

2.6. Transmission electron microscopy (TEM) and atomic force microscopy (AFM)

Suspensions of never-dried samples (0.05 wt%) were dropped onto a carbon-coated Cu grid, which was hydrophilized by plasma treatment. Excess dispersion was removed using a filter paper, followed by air drying. The samples were observed using TEM (JEM-1400, JEOL, Japan) at an acceleration voltage of 100 kV. Suspensions of the never-dried samples (0.01–0.05 wt%) were applied to freshly cleaved mica, followed by vacuum drying at 23 °C. The samples were observed using AFM (SPM-9600, Shimadzu, Japan) with a Si cantilever (OMCL-AC240TS, Olympus, Japan) in a dynamic mode. Images were acquired with a scanning area of 5 × 5 μm^2 and 1024 × 1024 pixels.

2.7. Small-angle X-ray scattering (SAXS) and wide-angle X-ray diffraction (WAXD)

Suspensions of never-dried samples were mixed with 10 % polyvinyl alcohol (PVA) to obtain a final PVA-to-sample solid content ratio of 3:2. The mixture was cast and dried at 35 °C to obtain thin-film samples. Synchrotron X-ray diffraction measurements were performed at beamline BL40B2 at the SPring-8 facility (Japan). X-rays (wavelength = 1.0 Å) were irradiated orthogonal to the film thickness direction. The diffraction patterns were recorded on hybrid photon-counting detectors (PILATUS 2 M and EIGER2 S 500 K, Dectris, Switzerland) with camera lengths of 3.0 and 0.1 m for SAXS and WAXD, respectively. The camera lengths were calibrated using AgBeH powder.

3. Results and discussion

3.1. Chemical structures of synthetic cellulose oligomers

Except for primer **10**, precipitation for all other primers occurred after an incubation period of three days. The precipitates were collected as synthetic products obtained from each primer and subjected to various analyses. The synthetic products of primers **1–9** (hereafter designated as oligomers **1–9**) were dissolved in 2 % LiCl/DMSO at 23 °C

and subsequently subjected to ^{1}H NMR spectroscopy (Fig. 3a). All proton peaks in the cellulose oligomers were assigned based on our previous study (Sasaki et al., 2024), matching the NMR spectra obtained for oligomers **1** and **2**. For the other spectra, the peaks derived from the OH protons in α and β anomeric configuration at the reducing end (6.48 and 6.78 ppm) disappeared. Peaks derived from the alkyl chain (< 2 ppm) and aromatic rings (> 6.5 ppm) were observed in the spectra of oligomers **5** and **6–8**, respectively. However, for oligomer **3**, negligible peaks from the OH protons in the α and β anomeric configuration at the reducing ends were observed, indicating contamination of the synthetic product without a methyl group at the reducing ends. As described later, primer **3** has low CDP activity; thus, αG1P produced by SP in the reaction system was not immediately consumed for synthesis but was hydrolyzed to glucose, which acts as a primer, synthesizing cellulose oligomers without functional groups. These side reactions have been previously reported (Samain et al., 1995).

The addition of functional groups at the reducing ends did not affect most of the proton peaks derived from OH and CH in the glucose rings of the internal residues and non-reducing ends, maintaining the same features as those of the cellulose oligomers without any functional groups (Fig. 3a). However, the peaks at the reducing ends shifted. Therefore, we assigned these peaks using various two-dimensional NMR spectroscopic methods, including heteronuclear single quantum coherence (HSQC)-total correlation spectroscopy (TOCSY), TOCSY, correlation spectroscopy (COSY), and heteronuclear multiple-bond correlation (HMBC) (see Supplementary Information for details). The peaks attributed to the protons at the C1 position of the reducing ends (designated R1) are shown in Fig. 3a (arrowheads). For oligomers **6–9**, additional peaks appear near the proton peaks at the C1 position of the internal glucose residue, which are derived from the proton at the C1 position of the internal glucose residue adjacent to the reducing end (designated as R'1) (Fig. 3a, inset). Notably, in oligomers containing aromatic rings (**6–8**), the R1 peaks exhibit a more pronounced shift from the peaks of the internal residues and non-reducing ends. The R'1 peaks are clearly separated from those of the internal residues owing to the significant magnetic anisotropy of aromatic rings, inducing strong changes in the electronic environment of adjacent glucose residues. Compared to those in oligomer **6**, the R1 and R'1 peaks in oligomers **7** and **8** shift to higher and lower magnetic fields, respectively, which is consistent with the electron-donating and electron-withdrawing effects of the hydroxyl and nitro groups on the aromatic ring, respectively.

The FT-IR spectra of the synthesized products are shown in Fig. 3b. Typical cellulose spectra were obtained for all the synthetic products. Functional groups without protons, nitro groups, or azido groups are confirmed and could not be directly observed by ^{1}H NMR. For oligomers **8** and **9**, peaks derived from the nitro (1530 cm^{-1}, asymmetric stretching vibration; 1350 cm^{-1}, symmetric stretching vibration) and azido groups (2090 cm^{-1}) are observed, respectively. Furthermore, peaks derived from the aromatic ring (1400–1600 cm^{-1}: CC skeletal vibration, 700–900 cm^{-1}: CH out-of-plane bending vibration) are observed for oligomers **6–8**. Peaks derived from CH (3000–2800 cm^{-1}) for oligomer **5** are broader than those of other oligomers, indicating the presence of an alkyl chain. Differences in the crystalline forms of cellulose are also observed, as discussed in Section 3.3.

3.2. DP and yield of synthetic cellulose oligomers

The number-averaged DP (DPn) of each cellulose oligomer was calculated as the ratio of the areas of the terminal and internal peaks in the ^{1}H NMR spectra (Table 1). Details of the peak positions in the NMR spectra used in the calculations are provided in the Supplementary Information. Furthermore, the DP was measured using MALDI-TOF MS, and the resulting spectra are shown in Fig. 4. The observed peaks correspond to either sodium ion (Na^{+}) or potassium ion (K^{+}) adducts of the oligomers, with an interval of 162 Da corresponding to glucose residues. In addition to the Na^{+} and K^{+} adducts, the spectrum of oligomer **8** exhibits numerous peaks corresponding to the Na^{+} and K^{+}

Table 1
Number-averaged degree of polymerization (DPn) and yield of cellulose oligomers **1–9** as well as CDP activity of primers **1–9**.

Primer/ Oligomer	DP_n (NMR)	DP_n (MALDI-TOF MS)	Yield (%)	CDP activity (mM/sec)
1	7.36	8.07	9.71	6.51×10^{-5}
2	6.68	6.78	32.40	1.66×10^{-3}
3	14.68	9.56	1.95	6.70×10^{-6}
4	7.56	7.69	11.95	4.99×10^{-5}
5	6.52	6.88	16.51	7.57×10^{-4}
6	6.28	6.92	26.65	4.96×10^{-4}
7	6.16	6.54	25.36	5.89×10^{-4}
8	6.15	5.98	25.58	6.82×10^{-4}
9	7.03	7.34	18.42	1.58×10^{-4}

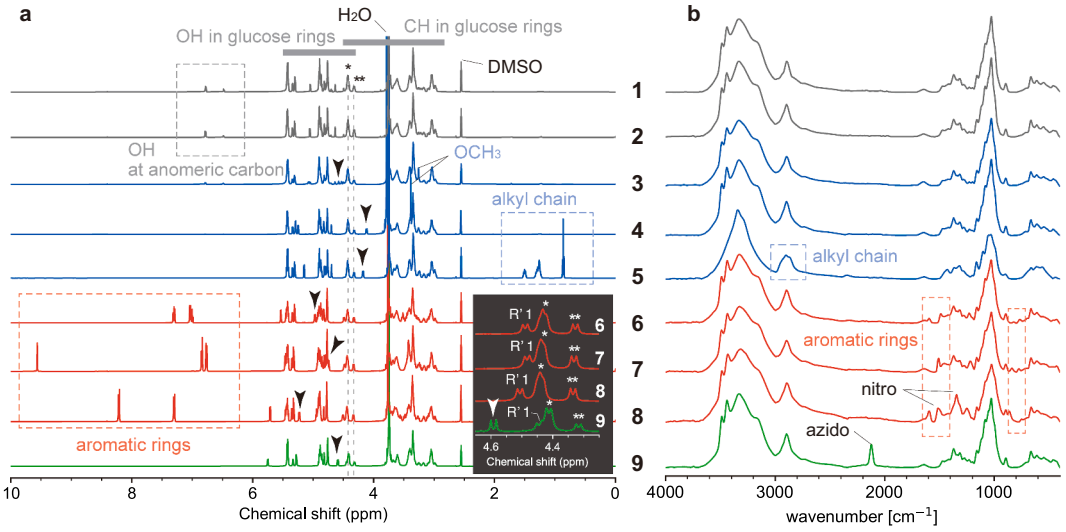

Fig. 3. (a) ^{1}H NMR and (b) FT-IR spectra of oligomers **1–9**. In (a), the arrowheads indicate the peaks from CH protons at C1 of the reducing ends (R1), and * and ** indicate peaks from CH protons at C1 of the internal residue and non-reducing end, respectively. The inset in (a) shows enlarged spectra of oligomers **6–9**, with the appearance of peaks of CH protons at C1 of the internal residues (*), non-reducing ends (**), reducing ends (arrowheads), and internal residues adjacent to the reducing ends (R'1).

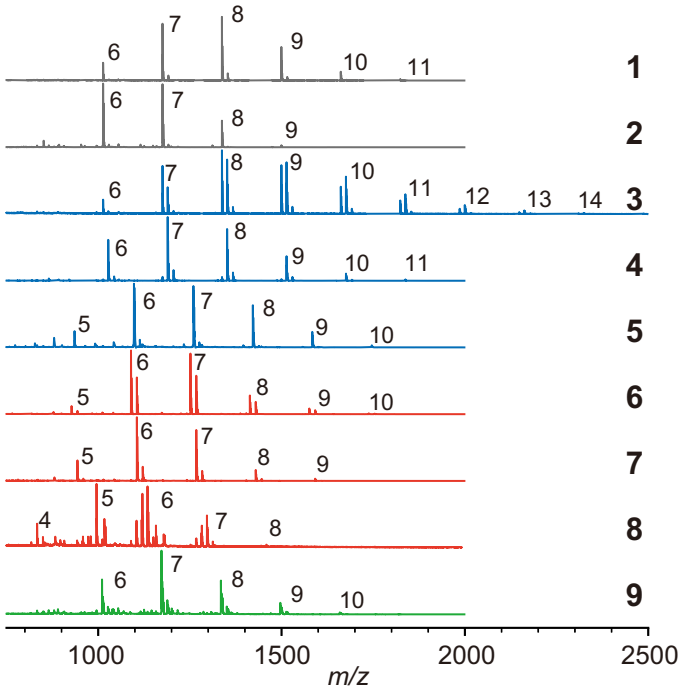

Fig. 4. MALDI-TOF MS spectra of cellulose oligomers **1**–**9**. The numbers indicate their DP.

adducts of oxygen elimination and NH_2 radical reaction products (Ueda et al., 2007). For oligomer **9**, the peaks corresponding to the Na^+ and K^+ adducts of the N_2 elimination products are also observed. The number-average molecular weight (Mn), weight-average molecular weight (Mw), and polydispersity index (Mn/Mw) were calculated from these peaks (see Supplementary Information for details). The DPn values are listed in Table 1. The DPn values calculated by NMR and MALDI-TOF MS are similar, except for that of oligomer **3**, which contains a high proportion of contaminating oligomers without functional groups at the reducing ends. Given that the terminal peaks of these oligomers were not considered, the NMR DPn values were likely overestimated.

Cellulose generally becomes insoluble and precipitates when a DP of 6 or higher is obtained. For oligomers **5**–**8**, peaks corresponding to a DP of 5 or lower are clearly observed, which can be ascribed to a decreased solubility due to the alkyl chains or aromatic rings present at the reducing ends. From the weights of the synthesized products and the DPn calculated using MALDI-TOF MS, the molar conversion rate of the donor (sucrose in this study) into the synthesized products was calculated as the yield (Table 1), using the following equation:

$$\text{Yield } (\%) = \frac{\text{Moles of glucose units in the synthesized product}*}{\text{Moles of sucrose used}} \times 100$$

*Excluding the reducing-end moiety derived from the primer.

Primer **2** affords the highest yield, exceeding 30 %, indicating highly efficient synthesis. The yield is inversely correlated with the DP.

3.3. Relationship among CDP activity, yield, and DP

The CDP activity, as evaluated by the amount of phosphate released, is shown in Table 1. CDP primarily degrades cellulose oligomers into cellobiose; thus, the activity of glucose in the synthetic direction is considerably lower than that of cellobiose (Hiraishi et al., 2009). A difference of >100 times between the activity values for glucose (primer **1**) and cellobiose (primer **2**) is observed. Primer **4** displays almost the same activity as glucose (primer **1**), whereas primer **3** exhibits approximately 1/10 of the activity. The decreased activity against α-linkages is consistent with the inherent substrate specificity of CDP for cellobiose. Similarly, no precipitation is observed for primer **10**, indicating the importance of conformation of the linkage from anomeric carbon. Primer **9** exhibits approximately 2.5 times the activity of glucose (primer **1**), suggesting a negligible effect of the oxygen directly linked to anomeric carbon. Furthermore, primer **5** and the three aromatic primers **6**–**8** exhibit significantly higher activity than glucose (primer **1**) and approximately half that of cellobiose (primer **2**). Thus, even if the structure of the functional group linked to glucose via a β-bond differs from glucose, the CDP activity can still be enhanced as long as it does not interfere with the CDP binding. Among the three primers containing aromatic rings (primers **6**–**8**), primer **8**, which is used as a model substrate for the measurement of β-glucosidase activity, exhibit the highest value.

Fig. 5a shows a plot of yield against CDP activity. The yield increases logarithmically with CDP activity. Although the kinetics is difficult to discuss given the multiple steps involved, such as G1P production by SP, chain elongation, and crystallization of the elongated molecular chains, CDP activity governs the yield of the synthetic products. However, primer **5** deviates from this trend and results in a lower yield. As discussed later, the crystal structure of oligomer **5** is different from that of the other oligomers, suggesting that the crystallization behavior affects the yield.

Fig. 5b and 5c show the CDP activity in relation to DPn and polydispersity, respectively. Oligomers synthesized from glucose by CDP possess higher DP and polydispersity than those synthesized from cellobiose, as explained by the difference in CDP activity toward the primers (Hiraishi et al., 2009; Serizawa et al., 2017). According to this mechanism, primers with low CDP activity achieve minimal synthesis of disaccharides from monosaccharide primers. These disaccharides then preferentially elongate, and fully elongated oligomers precipitate. In the initial stages of the reaction, only a few dissolved oligomer chains were present in the system, delaying precipitation and increasing the DP. In the later stages of the reaction, more dissolved substances are present in the system, prompting an earlier precipitation of oligomers, decreasing the average DP, and broadening the molecular weight distribution (Serizawa et al., 2017). The results of the current study are consistent with this mechanism. Therefore, despite the differences in primer structure, the primary mechanism, which can be explained by

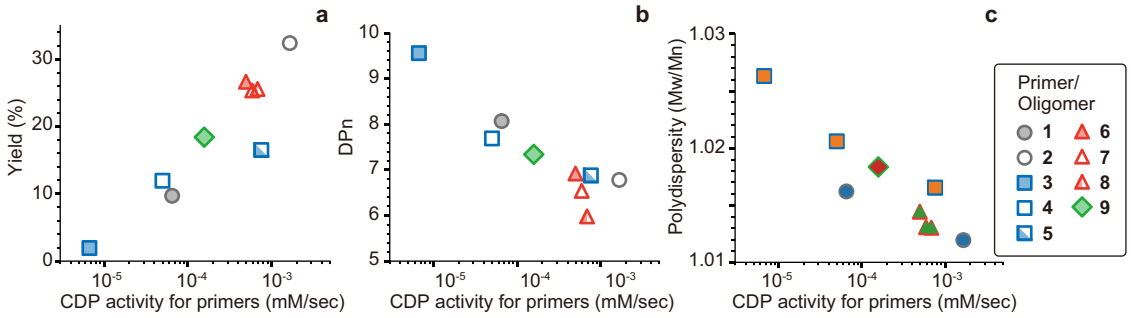

Fig. 5. CDP activity for primers **1**–**9** vs. (a) yield, (b) DPn, and (c) polydispersity of oligomers **1**–**9**.

differences in CDP activity, remains valid. However, primers containing aromatic rings (primers **6**–**8**) tended to exhibit lower DP owing to solubility effects.

3.4. Crystalline shapes and forms

TEM images of the synthesized oligomers are shown in Fig. 6. Similar to previous studies, all the oligomers, except for oligomer **5,** form plate-like microcrystals of different sizes and shapes. Even for oligomers **1** and **2**, which do not contain any functional groups, the microcrystal sizes are significantly different. Oligomer **2** frequently exhibits small microcrystals, forming bundles by twisting, which is similar to reports of chemically synthesized cellulose oligomers with DP = 6 (Fittolani et al., 2022). For oligomers **3, 4**, and **9**, which display relatively high DPn values, larger plate-like crystals, similar to those of primer **1**, are observed. The widths of these crystals vary widely, ranging from 100 nm to 1 μm. In contrast, the cellulose oligomers containing aromatic rings (oligomers **6**–**8**) exhibit smaller and thinner crystals. The widths of most of these crystals are <200 nm. These findings indicate that the size of the plate-like crystals is influenced by both the functional groups introduced on the surface and the DP. An additional hypothesis is that the CDP activity, which is correlated with the DP, affects the crystal size. Generally, slower crystallization results in the formation of larger crystals. With low CDP activity, the crystallization process tends to be slower and can lead to the formation of larger crystals. For oligomer **5**, twisted microcrystals are observed, which is consistent with previous reports (Serizawa et al., 2021; Yataka et al., 2016).

Fig. 7 shows the WAXD and SAXS patterns and profiles of the cast films prepared by mixing the cellulose oligomer suspensions and PVA with incident X-rays perpendicular to film thickness. All oligomers, except for oligomer **5**, exhibit arc-shaped SAXS and WAXD patterns (Fig. 7a) owing to the flat-on orientation of the plate-like microcrystals during the film-drying process. In contrast, oligomer **5** exhibits mostly ring-shaped diffraction WAXD and SAXS patterns, with some degree of orientation observed in SAXS. This can be ascribed to the formation of twisted microcrystals of oligomer **5**.

The WAXD profiles of all oligomers, except for oligomer **5**, exhibit three diffraction peaks at the scattering vector Q = 8.5, 14.3, and 15.3 nm^{-1}, which are typical for cellulose II structures (Fig. 7b). In contrast, oligomer **5** displays a typical cellulose I diffraction profile with three diffraction peaks at Q = 10.5, 11.6, and 16.1 nm^{-1}, consistent with previous reports (Serizawa et al., 2021; Yataka et al., 2016). In the FT-IR spectra (Fig. 3b), two characteristic peaks of cellulose II (3490 and 3440 cm^{-1}) are observed for all oligomers, except for oligomer **5**, which has a characteristic cellulose I peak (3340 cm^{-1}), in agreement with the WAXD results.

3.5. Relationship between DP and thickness of plate-like crystals

The SAXS profiles (Fig. 7c) display a single peak at Q = 1–1.5 nm^{-1} for all samples, except for oligomer **5**. The thicknesses calculated from the peak tops are listed in Table 2. This peak corresponds to the periodicity derived from the thickness of the plate-like crystals (Wada et al., 2021). In contrast, oligomer **5** exhibits a peak at lower Q values, in addition to the peak observed at the same position as the other samples.

The thicknesses of the plate-like crystals were measured using AFM (Fig. 8 and S19). The height profiles of the regions without an overlap in the plate-like crystals are almost constant, and the average value was calculated as the thickness of the plate-like crystals (Table 2). These values are consistent with those obtained by SAXS. Although the films used for the SAXS measurements are composites of PVA, the thickness of the PVA between the crystals is considered negligible. For oligomer **5**, periodic roughness is observed, corresponding to the twisting, and the height of the concave parts is 8.71 nm, which is consistent with the thickness obtained from the low-Q peak in the SAXS profile (Fig. 7c, 5)

The thickness of the plate-like crystals was estimated from the DPn calculated using MALDI-TOF MS. As shown in Fig. 9a, the calculation method assumes that the molecular chains has a rounded DPn value and calculates the length in the molecular chain direction when forming cellulose II crystals. Functional groups were not included in the

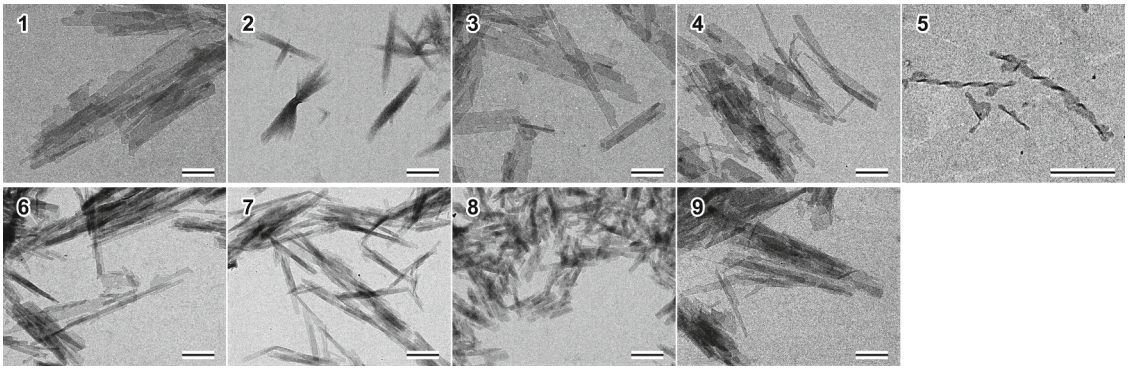

Fig. 6. TEM images of oligomers **1**–**9**. Scale bar = 1 μm. Magnification: 5000 × (except for oligomer **5**, which was taken at 10,000 ×).

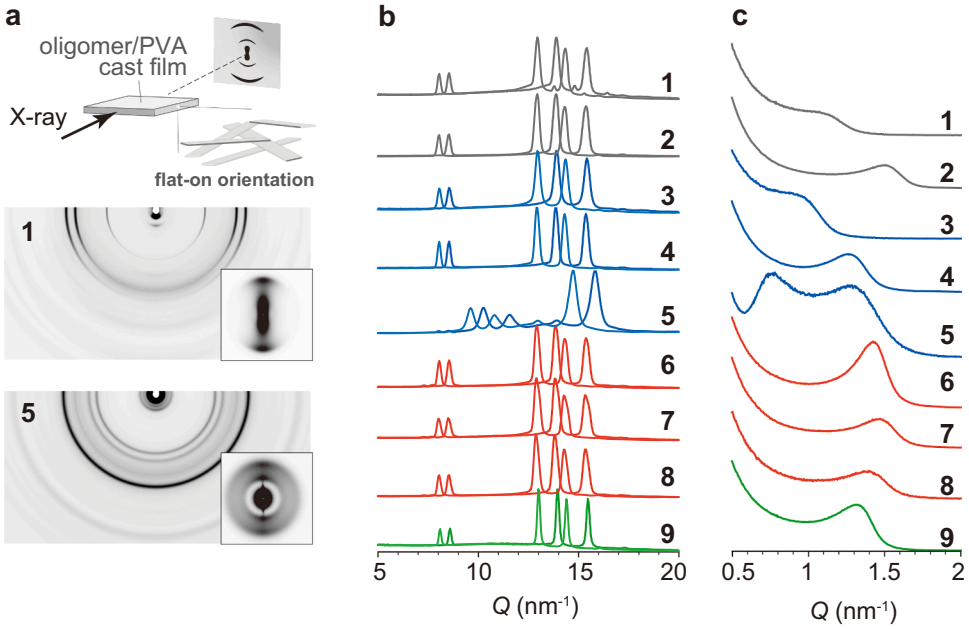

Fig. 7. WAXD and SAXS patterns and profiles of cellulose oligomer/PVA films. (a) WAXD and SAXS (inset) patterns of oligomer films **1** and **5**. As illustrated in (a), the film thickness direction is vertical to the patterns. (b) WAXD profiles of the films with oligomers **1**–**9**, obtained from the horizontal direction of the WAXD patterns. (c) SAXS profiles of the films with oligomers **1**–**9**, obtained from the vertical direction of the SAXS patterns.

Table 2
Thickness of the plate-like crystals calculated by SAXS and AFM.

Oligomer	SAXS (nm)	AFM (nm)
1	5.28	5.37
2	4.19	4.44
3	6.10	6.11
4	4.95	4.42
5	4.59 / 8.46	8.71
6	4.40	4.36
7	4.31	4.66
8	4.55	4.23
9	4.79	4.13

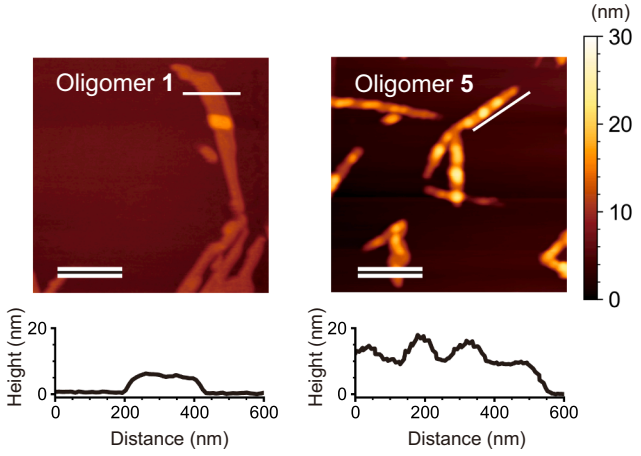

Fig. 8. AFM images (upper) and height profiles (bottom) of oligomers **1** and **5**. Height profiles are obtained from the white lines in the images, but the line is offset from the sample in the image of oligomer **5**. Scale bar = 500 nm.

calculations. The thickness calculated from the SAXS exceed the values estimated from DPn by approximately 0.5 nm for most samples (Fig. 9b). The higher measured values compared to the estimated values based on DPn are ascribed to the presence of longer molecular chains than those used in the calculations. In particular, a large difference is observed for oligomer **3**, which also possesses high polydispersity, supporting this explanation. However, for oligomer **8**, the measured value exceeds the estimated value by >1 nm, which is attributed to the influence of the longer molecular chains and the size of the aromatic rings on the crystal surface. As shown in Fig. 9c, the surface functional groups adopt two major arrangements. For type A, the addition of aromatic rings has a minimal effect on the thickness, whereas for type B, the size of the aromatic rings, assumed to be 0.28 nm each, can increase the thickness by up to 0.56 nm. Therefore, for oligomer **8**, the arrangement likely corresponds to type B, which matches the measured values more closely. In contrast, for oligomers **6** and **7**, assuming type B would result in measured values that are almost equal to or slightly lower than the estimated values, making type A a more appropriate assumption. For oligomer **5**, a model has been proposed in which the oligomer chains are aligned parallel to the alkyl chains, facing each other (Yataka et al., 2016). The data obtained in the current study are consistent with this model (Figure S20). Specifically, the crystal thickness of the two oligomer chains corresponds to the height of the concave parts observed by AFM and the low-*Q* peak observed by SAXS. In contrast, the high-*Q* peak observed using SAXS is almost identical to the length of the oligomer chains, reflecting this periodicity.

4. Conclusion

In this study, we characterized cellulose oligomers synthesized by CDP using different primers. The resulting yields and DP values were primarily influenced by differences in the CDP activity of the primers, regardless of whether functional groups were introduced at their reducing ends. In other words, primers with higher CDP activity tended to result in higher yields and lower DP. Solubility was also recognized as a key factor in determining DP, with primers containing alkyl chains or aromatic rings typically leading to a lower DP.

The synthesized products mostly consisted of plate-like crystals with thicknesses corresponding to the molecular chain lengths calculated from the DP. The lateral size of the crystals tended to increase with increasing DP. An exception was the primer bearing an alkyl chain,

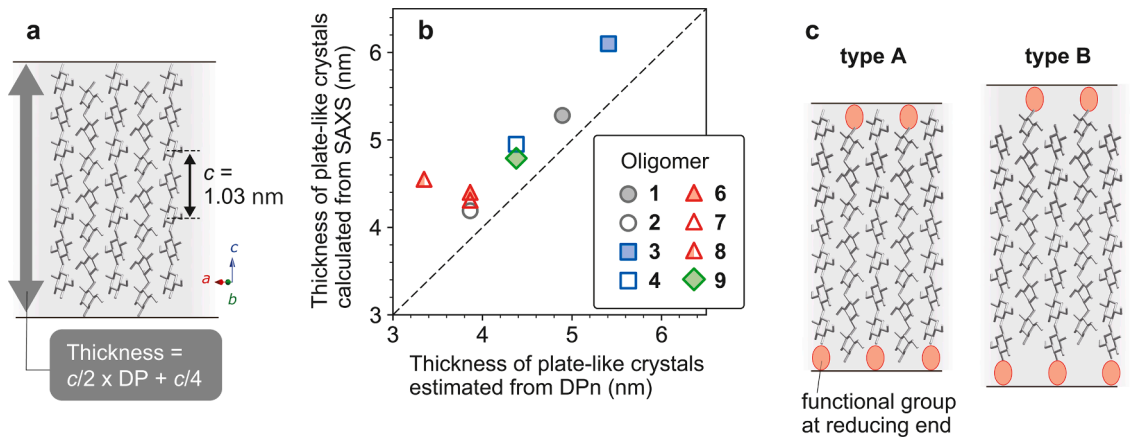

Fig. 9. Relationship between the thickness of plate-like crystals (oligomers **1**–**4** and **6**–**9**) and DP. (a) Calculation method of the thickness of the plate-like crystals based on DP (rounded DPn values obtained by MALDI-TOF MS were used as DP). (b) Calculated versus measured thicknesses of the plate-like crystals. (c) Two possible positions of functional groups at the reducing ends.

which exhibited a twisted crystal structure containing cellulose I.

Although the synthesis conditions were kept constant in this study, varying the temperature and substrate concentration is known to enable the control of both DP and crystal size. Therefore, regardless of the primer structure, the DP of synthetic cellulose oligomers and the size of their plate-like crystals can be controlled by tuning these conditions. The applicability of such a simple strategy is highly advantageous for expanding the utilization of cellulose oligomers synthesized by CDP. This tunability could be utilized to explore how different structural features influence dispersion properties and solubility in various solvents.

Funding

This work was supported by JST CREST, Japan [grant number JPMJCR22L3], and JSPS KAKENHI grants [grant numbers 19H03018, 20H03043, 21H04733, and 23H02276] from the Japan Society for the Promotion of Science.

Data statement

The data used in this study are provided in the text and the Supporting Information.

CRediT authorship contribution statement

Tatsuhiro Konishi: Writing – original draft, Investigation, Formal analysis. **Atsushi Sasaki:** Investigation, Formal analysis. **Ryosuke Kusumi:** Validation, Funding acquisition. **Masahisa Wada:** Validation, Supervision, Funding acquisition, Conceptualization. **Kayoko Kobayashi:** Writing – review & editing, Validation, Funding acquisition, Formal analysis, Conceptualization.

Declaration of competing interest

The authors declare that they have no known competing financial interests or personal relationships that could have appeared to influence the work reported in this paper.

Acknowledgments

The synchrotron radiation experiments were performed at BL40B2 of SPring-8 with the approval of the Japan Synchrotron Radiation Research Institute (JASRI) (Proposal Nos. 2022A1487 and 2023B1402). This work was partially supported by the North Campus Instrumental Analysis Station at Kyoto University. The authors also thank Dr. Satoshi Kimura from the University of Tokyo for preparing the recombinant CDP.

Supplementary materials

Supplementary material associated with this article can be found, in the online version, at doi:10.1016/j.carpta.2025.100731.

Data availability

Data will be made available on request.

References

Adharis, A., Petrović, D. M., Özdamar, I., Woortman, A. J. J., & Loos, K. (2018). Environmentally friendly pathways towards the synthesis of vinyl-based oligocelluloses. *Carbohydrate Polymers, 193*, 196–204. https://doi.org/10.1016/j.carbpol.2018.03.098

Arai, M., Tanaka, K., & Kawaguchi, T. (1994). Purification and properties of cellodextrin phosphorylase from *Clostridium thermocellum*. *Journal of Fermentation and Bioengineering, 77*, 239–242. https://doi.org/10.1016/0922-338X(94)90226-7

de Andrade, P., Muñoz-García, J. C., Pergolizzi, G., Gabrielli, V., Nepogodiev, S. A., Iuga, D., Fábián, L., Nigmatullin, R., Johns, M. A., Harniman, R., Eichhorn, S. J., Angulo, J., Khimyak, Y. Z., & Field, R. A. (2021). Chemoenzymatic synthesis of fluorinated cellodextrins identifies a new allomorph for cellulose-like materials. *Chemistry (Weinheim an Der Bergstrasse, Germany), 27*, 1374–1382. https://doi.org/10.1002/chem.202003604

Fittolani, G., Vargová, D., Seeberger, P. H., Ogawa, Y., & Delbianco, M. (2022). Bottom-up approach to understand chirality transfer across scales in cellulose assemblies. *Journal of the American Chemical Society, 144*, 12469–12475. https://doi.org/10.1021/jacs.2c04522

Guberman, M., & Seeberger, P. H. (2019). Automated glycan assembly: A perspective. *Journal of the American Chemical Society, 141*, 5581–5592. https://doi.org/10.1021/jacs.9b00638

Hata, Y., Sawada, T., Marubayashi, H., Nojima, S., & Serizawa, T. (2019). Temperature-directed assembly of crystalline cellulose oligomers into kinetically trapped structures during biocatalytic synthesis. *Langmuir: The ACS Journal of Surfaces and Colloids, 35*, 7026–7034. https://doi.org/10.1021/acs.langmuir.9b00850

Hiraishi, M., Igarashi, K., Kimura, S., Wada, M., Kitaoka, M., & Samejima, M. (2009). Synthesis of highly ordered cellulose II in vitro using cellodextrin phosphorylase. *Carbohydrate Research, 344*(18), 2468–2473. https://doi.org/10.1016/j.carres.2009.10.002

Kita, Y., Kusumi, R., Kimura, T., Kitaoka, M., Nishiyama, Y., & Wada, M. (2020). Surface structural analysis of selectively 13C-labeled cellulose II by solid-state NMR spectroscopy. *Cellulose (London, England), 27*, 1899–1907. https://doi.org/10.1007/s10570-019-02896-x

Kobayashi, S., Kashiwa, K., Kawasaki, T., & Shoda, S. (1991). Novel method for polysaccharide synthesis using an enzyme: The first in vitro synthesis of cellulose via a nonbiosynthetic path utilizing cellulase as catalyst. *Journal of the American Chemical Society, 113*, 3079–3084. https://doi.org/10.1021/ja00008a042

Krishnareddy, M., Kim, Y.-K., Kitaoka, M., Mori, Y., & Hayashi, K. (2002). Cellodextrin phosphorylase from clostridium thermocellum YM4 strain expressed in *Escherichia coli*. *Journal of Applied Glycoscience, 49*, 1–8. https://doi.org/10.5458/jag.49.1

Nakatsubo, F., Kamitakahara, H., & Hori, M. (1996). Cationic ring-opening polymerization of 3,6-di-O-benzyl-α-d-glucose 1,2,4-orthopivalate and the first chemical synthesis of cellulose. *Journal of the American Chemical Society, 118*, 1677–1681. https://doi.org/10.1021/ja953286u

Nohara, T., Sawada, T., Tanaka, H., & Serizawa, T. (2017). Enzymatic synthesis and protein adsorption properties of crystalline nanoribbons composed of cellulose oligomer derivatives with primary amino groups. *Journal of Biomaterials Science. Polymer Edition, 28*, 925–938. https://doi.org/10.1080/09205063.2017.1322248

Petrović, D. M., Kok, I., Woortman, A. J. J., Ćirić, J., & Loos, K. (2015). Characterization of oligocellulose synthesized by reverse phosphorolysis using different cellodextrin phosphorylases. *Analytical Chemistry, 87*, 9639–9646. https://doi.org/10.1021/acs.analchem.5b01098

Pylkkänen, R., Maaheimo, H., Liljeström, V., Mohammadi, P., & Penttilä, M. (2024). Glycoside phosphorylase catalyzed cellulose and β-1,3 glucan synthesis using chromophoric glycosyl acceptors. *Biomacromolecules, 25*, 5048–5057. https://doi.org/10.1021/acs.biomac.4c00455

Pylkkänen, R., Mohammadi, P., Arola, S., de Ruijter, J. C., Sunagawa, N., Igarashi, K., & Penttilä, M. (2020). In vitro synthesis and self-assembly of cellulose II nanofibrils catalyzed by the reverse reaction of Clostridium thermocellum cellodextrin phosphorylase. *Biomacromolecules, 21*(10), 4355–4364. https://doi.org/10.1021/acs.biomac.0c0116

Saheki, S., Takeda, A., & Shimazu, T. (1985). Assay of inorganic phosphate in the mild pH range, suitable for measurement of glycogen phosphorylase activity. *Analytical Biochemistry, 148*(2), 277–281. https://doi.org/10.1016/0003-2697(85)90229-5

Samain, E., Lancelon-Pin, C., Férigo, F., Moreau, V., Chanzy, H., Heyraud, A., & Driguez, H. (1995). Phosphorolytic synthesis of cellodextrins. *Carbohydrate Research, 271*, 217–226. https://doi.org/10.1016/0008-6215(95)00022-L

Sasaki, A., Konishi, T., Kobayashi, K., Wada, M., & Kusumi, R. (2024). Complete 1H and 13C NMR assignment of cellulose oligomer in LiCl/DMSO. *Cellulose (London, England)*, 1–10. https://doi.org/10.1007/s10570-024-06089-z

Serizawa, T., Fukaya, Y., & Sawada, T. (2017). Self-assembly of cellulose oligomers into nanoribbon network structures based on kinetic control of enzymatic oligomerization. *Langmuir: The ACS Journal of Surfaces and Colloids, 33*, 13415–13422. https://doi.org/10.1021/acs.langmuir.7b03653

Serizawa, T., Kato, M., Okura, H., Sawada, T., & Wada, M. (2016). Hydrolytic activities of artificial nanocellulose synthesized via phosphorylase-catalyzed enzymatic reactions. *Polymer Journal, 48*, 539–544. https://doi.org/10.1038/pj.2015.125

Serizawa, T., Tanaka, S., & Sawada, T. (2021). Control of parallel versus antiparallel molecular arrangements in crystalline assemblies of alkyl β-cellulosides. *Journal of Colloid and Interface Science, 601*, 505–516. https://doi.org/10.1016/j.jcis.2021.05.117

Serizawa, T., Yamaguchi, S., Sugiura, K., Marten, R., Yamamoto, A., Hata, Y., Sawada, T., Tanaka, H., & Tanaka, M. (2024). Antibacterial synthetic nanocelluloses synergizing with a metal-chelating agent. *ACS Applied Bio Materials, 7*, 246–255. https://doi.org/10.1021/acsabm.3c00846

Sheth, K., & Alexander, J. K. (1969). Purification and properties of β-1,4-oligoglucan: Orthophosphate glucosyltransferase from *Clostridium thermocellum*. *The Journal of Biological Chemistry, 244*, 457–464. https://doi.org/10.1016/s0021-9258(18)94451-0

Sugiura, K., Saito, M., Sawada, T., Tanaka, H., & Serizawa, T. (2022). Cellodextrin phosphorylase-catalyzed single-process production and superior mechanical properties of organic–inorganic hybrid hydrogels composed of surface-carboxylated synthetic nanocelluloses and hydroxyapatite. *ACS Sustainable Chemistry & Engineering, 10*, 13484–13494. https://doi.org/10.1021/acssuschemeng.2c04349

Ueda, K., Katagiri, T., Shimada, T., Irie, S., Sato, T.-A., Nakamura, Y., & Daigo, Y. (2007). Comparative profiling of serum glycoproteome by sequential purification of glycoproteins and 2-nitrobenzensulfenyl (NBS) stable isotope labeling: A new approach for the novel biomarker discovery for cancer. *Journal of Proteome Research, 6*, 3475–3483. https://doi.org/10.1021/pr070103h

Wada, M., Wakiya, S., Kobayashi, K., Kimura, S., Kitaoka, M., Kusumi, R., Kimura, F., & Kimura, T. (2021). Three-dimensional alignment of cellulose II microcrystals under a strong magnetic field. *Cellulose (London, England), 28*, 6757–6765. https://doi.org/10.1007/s10570-021-03954-z

Wang, Y., Li, Q., Shao, T., Miao, W., You, C., & Wang, Z. (2022). Fabrication of anti-fouling and anti-bacterial hydrophilic coating through enzymatically-synthesized cellooligomers. *Applied Surface Science, 600*, Article 154133. https://doi.org/10.1016/j.apsusc.2022.154133

Yataka, Y., Sawada, T., & Serizawa, T. (2015). Enzymatic synthesis and post-functionalization of two-dimensional crystalline cellulose oligomers with surface-reactive groups. *Chemical Communications, 51*, 12525–12528. https://doi.org/10.1039/C5CC04378F

Yataka, Y., Sawada, T., & Serizawa, T. (2016). Multidimensional self-assembled structures of alkylated cellulose oligomers synthesized via in vitro enzymatic reactions. *Langmuir: The ACS Journal of Surfaces and Colloids, 32*, 42. https://doi.org/10.1021/acs.langmuir.6b02679

Zhang, Y.-H. P., & Lynd, L. R. (2004). Kinetics and relative importance of phosphorolytic and hydrolytic cleavage of cellodextrins and cellobiose in cell extracts of *Clostridium thermocellum*. *Applied and Environmental Microbiology, 70*, 1563–1569. https://doi.org/10.1128/AEM.70.3.1563-1569.2004

Zhong, C., & Nidetzky, B. (2022). Precision synthesis of reducing-end thiol-modified cellulose enabled by enzyme selection. *Polymer Journal, 54*, 551–560. https://doi.org/10.1038/s41428-021-00599-4